

Deformable Strain Sensors Based on Patterned MWCNTs/ Polydimethylsiloxane Composites

Wenjun Xu,¹ Mark G. Allen²

¹School of Material Science and Engineering, Georgia Institute of Technology, Atlanta, Georgia 30332

²School of Electrical and Computer Engineering, Georgia Institute of Technology, Atlanta, Georgia 30332

Correspondence to: W. J. Xu (E-mail: wxu3@gatech.edu)

Received 27 May 2013; revised 18 July 2013; accepted 19 July 2013; published online 13 August 2013

DOI: 10.1002/polb.23361

ABSTRACT: Patterned MWCNT/polydimethylsiloxane (PDMS) nanocomposite strain sensors were achieved by a microelectromechanical system assisted electrophoretic deposition (EPD) technique. With the combined effect of superior intrinsic piezoresistivity of the individual MWCNT and the tunneling effect of the MWCNT network, the stretchable composite demonstrates high sensitivity to the tensile strain. The gauge factor shows a strong dependence on both the initial resistance of the CNT/PDMS composite and the applied strain level. The mechanism is elucidated by analyzing the structure-property-function of patterned CNT networks. When the entanglement of a MWCNT network allows effective load transfer, the sensitivity is primarily dominated by the intrinsic piezoresistivity of individual MWCNTs. Conversely, when the MWCNTs inter-

penetrate loosely, the tunneling effect prevails. The sensitivity of the device can be tailored by the proposed technique since MWCNT film thickness/density can be readily controlled by means of the patterning parameters of the EPD process. The work provides useful guidance for design and development of strain/stress sensors with targeted sensitivity for flexible electronics applications. © 2013 Wiley Periodicals, Inc. *J. Polym. Sci., Part B: Polym. Phys.* **2013**, *51*, 1505–1512

KEYWORDS: Carbon nanotube nanocomposite; conductive network; elastic nanocomposite; interpenetrating networks (IPN); microstructure; multiwalled carbon nanotubes; nanotechnology; Patterning; Piezoresistive strain sensors; Structure-properties relationship

INTRODUCTION The precise local pressure/strain monitoring is indispensable in the fields such as biomechanical implants, artificial skins, touch screens and structural health monitoring.^{1–3} As alternatives to traditional metal foil strain gauges and silicon piezoresistors, CNT/polymer composites take advantage of the high elasticity and low Young's modulus of the polymer and the superior piezoresistivity of CNTs. The piezoresistivity of the composite in general results from the combination of two effects: intrinsic piezoresistivity of the individual CNTs and the piezoresistivity induced by the tunneling resistance. Compared with spherical conductive fillers such as carbon black and silver nanoparticles, CNTs offer an additional benefit of possessing a very high intrinsic piezoresistivity, apart from acting only as a pure conductive path inside the polymer matrix. Under the sufficient amount of stress or strain, the hybridization of certain carbon atoms of CNTs can change from sp^2 to sp^3 , resulting in alterations of the band-gap energy and the electron transport property of a CNT, which leads to an extremely high gauge factor of up to 2900.^{4–6} Small band-gap semiconducting SWCNTs show a higher piezoresistivity than metallic or large band-gap semiconducting SWCNTs due to their potential to

achieve a larger alteration in band-gap openings,⁷ which indicates that the piezoresistivity can be tailored.

Another benefit CNT/polymer composites offer is the resistance change over a large strain range due to the low Young's modulus (few MPa) and the higher elasticity (>50%) of elastomeric polymers, in contrast with silicon and metals which typically have high Young's moduli of 20–100 GPa and the elastic elongation of less than 4%. The composite is capable of covering surfaces with arbitrary curvatures such as these in robots and human bodies, and thereby it becomes an attractive alternative for the next generation of highly sensitive, wide working range and large area flexible strain/stress sensors.

One key technical challenge of CNT sensors is how to allow the outstanding intrinsic piezoresistivity of nano-sized CNTs to take effect in microstructural and macrostructural component length scales, while simultaneously controlling the structure and assembly of the CNTs at the atomistic scale.⁸ To this end, sufficient load transfer from external strain/stress sources to an individual CNT is required, which can be partially fulfilled through a well-designed CNT network.

Therefore, the high and controlled sensitivity of a strain sensor can be achieved through the manipulation of the CNT network. Another challenge is how to accomplish micropatterning of CNT/polymer composites for microelectronics applications. In our previous study, a technique based on a microelectromechanical system (MEMS)-assisted electrophoretic deposition (EPD) and a transfer micromolding approach demonstrated to achieve the MWCNT/polymer micropatterning, while minimizing issues associated with the rheology and the dispersion of CNTs in polymer.^{9,10} In this work, this technique was further developed to achieve complex two-dimensional (2D)/three-dimensional (3D) CNT/polymer micropatterns and macropatterns with predictable CNT entanglement and thickness. The CNT/polydimethylsiloxane (PDMS) composite strain sensors developed in this work demonstrated high sensitivity. Intensive efforts in this article were made to elucidate piezoresistivity mechanisms of strain sensors based on specially patterned CNT network films. The sensing performance of sensors with a variety of the initial resistance was characterized and the correlation between the piezoresistivity and the CNT network properties was established. The resultant CNT composite sensors exhibited high sensitivities.

EXPERIMENTAL

Sample Preparation and Characterization

Patterned MWCNT/PDMS composites were fabricated through a MEMS-assisted EPD and transfer micromolding technique. MWCNT patterns with desired geometry and dimensions were first generated by selective assembly of acidified CNTs using the electric field onto a silicon template bearing desired electrode microstructures. The resultant MWCNT patterns were further transferred to a polymer matrix through transfer micromolding process, in which the prepolymers of PDMS (Sylgard 184, Dow Corning) were casted onto CNT patterns and cured. Upon demolding, the CNT patterns were transferred to the PDMS elastomeric matrix. Further details of the fabrication process can be obtained from literature reported previously.¹⁰ The specific design and fabrication of CNTs/PDMS microstructures for

evaluation of sensor performance are discussed in the subsequent device testing section.

Scanning electron microscopy (SEM) (Zeiss, Ultra60) was utilized to study the morphology of patterned MWCNT/PDMS composites and the CNT network. Raman spectroscopy (excitation wavelength: 488 nm) was exploited to probe the modification of the electronic structure in strained CNTs. The controlled strain was imparted to the CNT/PDMS composite through a micrometer attached to a stretching stage and the Raman spectrum was recorded immediately after each strain was imposed.

Test of the Sensitivity to the Tensile Strain

The piezoresistivity of the MWCNT/PDMS composite was characterized with a monotonic tensile testing in a Mini ElectroForce® 3100 Test Instruments (Bose). The MWCNT/PDMS composite used for the testing was produced from first depositing acidified CNTs into silicon patterns with the geometry illustrated in Figure 1(a) through MEMS-assisted EPD process under an electric field of 20 V cm^{-1} and MWCNT concentration of 0.1 g L^{-1} . At the bottom of silicon patterns, there was a 500-nm-thick gold layer deposited through the E-beam evaporation which served as the electrode for the CNT assembly. The CNT patterns generated inside the silicon trench were further transferred into a PDMS substrate through the aforementioned transfer micromolding process, which completed the fabrication of MWCNT/PDMS strain sensors. The details of fabrication parameters of four sensors tested in the work are summarized in Table 1. The two $2 \times 2 \text{ mm}^2$ CNT pads capping the 200- μm -wide and 1000- μm -long MWCNTs/PDMS microline were designed to create electrical connection from the microline to the external circuit. The two CNT pads were bonded to the gold-coated layer on the two ends of a polyurethane stretch frame with the CNT layer facing down to the frame. The center 1-mm-long microline was suspended over the 1-mm-wide gap of the frame [Fig. 1(b)]. Epoxy-based glue was further applied to encapsulate the entire nanocomposite to the stretch frame to ensure effective load transfer. The resistance readout was acquired through two metal

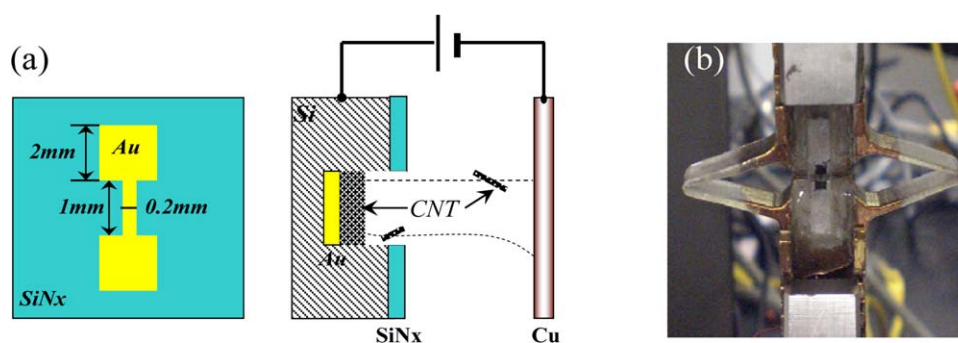


FIGURE 1 (a) Left: Scheme of the top view of the silicon template, right: scheme of the CNT patterning using MEMS assisted-EPD technique; (b) the digital image of the MWCNT/PDMS strain sensor in the sensitivity test system. [Color figure can be viewed in the online issue, which is available at wileyonlinelibrary.com.]

TABLE 1 Summary of Fabrication of Tested Sensors

Sensor No.	Electric Field of EPD ($V\text{ cm}^{-1}$)	Deposition Time of EPD (min)	CNT Film Thickness (μm)	R_0 of CNTs/PDMS ($M\Omega$)
1	20	2	0.6	462
2	20	4.5	0.9	380
3	20	5.5	1.8	161
4	20	7.5	2.8	83

wires bonded to the two ends of the frame using conductive silver epoxy. Monotonic tensile strain testing was then performed through a WinTest® digital control system and the resistance was recorded simultaneously using a multimeter connected to the metal wires.

RESULTS AND DISCUSSION

Morphology of the MWCNT/PDMS Composite

Figure 2 shows a variety of 2D/3D MWCNT patterns including microsprings, microcoils, and micropads ranging from micrometer to macrometer scale achieved on both plastic (polyolefin) and elastic (PDMS) substrates utilizing the proposed patterning technique. The MWCNT patterns exhibit both excellent flexibility and elasticity, and can be easily deformed to cover arbitrary curvatures [Fig. 2(b,c)]. The patterned CNT/PDMS composites can serve as multifunctional components in microsystems where flexibility is strongly desired, such as physical strain/stress sensors, artificial muscles/skins, bio-scaffolds, and foldable energy textiles.

Thickness Control of the Patterned CNT Network

As a strain-sensing element, entanglement of CNTs in the network is critical. One advantage the patterning technique in this work carries is the control of the thickness of the resultant CNT film, as EPD proves to be an effective approach to modulate the deposition rate and the deposition time, which directly impact the morphology of the assembled film. Equation (1) describes an approximate relationship between the deposited thickness and the parameters of EPD process according to Hamaker's law.¹¹

$$d = \frac{M}{\rho A} = (\alpha \mu c) \frac{E \cdot t}{\rho} \quad (1)$$

where d is deposited thickness, M is the total deposited mass, ρ is the mass density of the deposited film, A is the total area of the energized electrode, α is the mass fraction of the material deposited on a specific electrode, μ is the particle mobility in a given solution, c is the particle concentration in the dispersion, E is the applied electric field, and t is the deposition duration. d then can be controlled by varying E , c , and t . In the initial deposition stage, ρ increases with the electric field and time, so d may not increase linearly with E or t . When ρ approaches a constant, d is likely to increase linearly with E and t .

Though the precise equation has not yet been established for the deposition mass of CNTs in an EPD process due to the complexity of the system, the eq (1) was utilized to provide approximate theoretical predictions of the deposited thickness. In order to determine the value of α , the experimental value of the thickness at $E = 20\text{ V cm}^{-1}$, $t = 5\text{ min}$, and $c = 0.3\text{ g L}^{-1}$ was used, which was $2.59\text{ }\mu\text{m}$. The density $\rho = 1.23\text{ g cm}^{-3}$ and $\mu = 4.7 \times 10^{-4}\text{ cm}^2\text{ V}^{-1}\text{ s}^{-1}$ were obtained from literature,¹³ given the similarity of the two systems. The α was calculated to be 0.38. The values of α , ρ , c , and μ were further utilized to calculate the theoretical values of the deposited thickness under different electric fields and time duration. The prediction shows that the deposited CNT layer thickness exhibits a monotonic increase with the increase of both the deposition time and electric field, which is in good agreement with the experimental results as shown in Figure 3. The theoretically calculated values are close to the experimentally measured results. The technique can thereby be utilized to produce CNT sensors with a variety of initial resistance, which makes the mechanistic study of the device sensitivity possible in Piezoresistive Effects in MWCNT/PDMS Composites section.



FIGURE 2 (a) The optical image of CNT microspring patterns on PDMS, (b) the digital image of CNT patterns on a polyolefin film, and (c) the digital image of CNT patterns on a PDMS substrate. [Color figure can be viewed in the online issue, which is available at wileyonlinelibrary.com.]

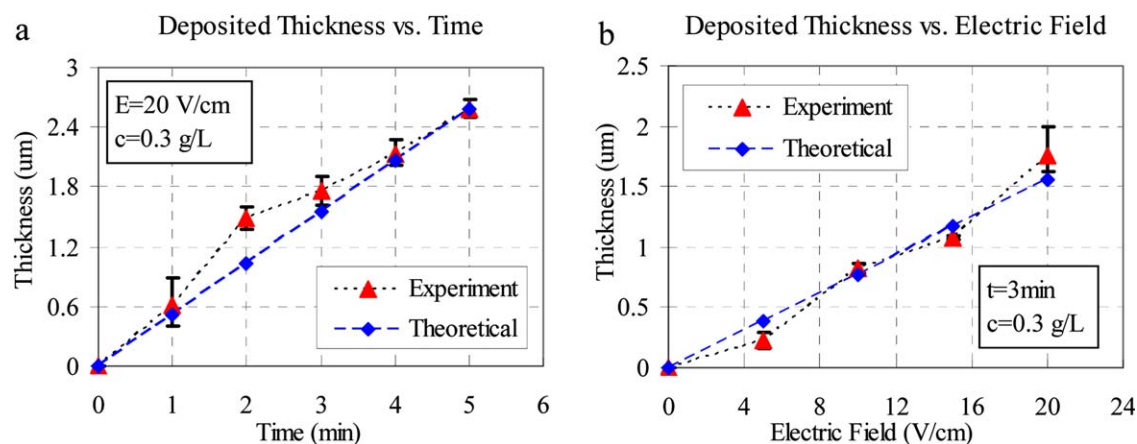


FIGURE 3 The CNT layer thickness as a function of: (a) the time under the constant E and c , and (b) the electric field under the constant c and t . Error bars show the deviation of the thickness. [Color figure can be viewed in the online issue, which is available at wileyonlinelibrary.com.]

Characterization of MWCNT/PDMS Strain Sensors

To investigate the strain sensitivity of the MWCNT/PDMS composites, a series of laboratory experiments were designed and undertaken. Four MWCNT/PDMS strain sensors with different initial resistances (R_0) as described in Table 1 were mechanically loaded under monotonic load patterns and characterized under the same experimental conditions. The R_0 can be conceptualized as a measurable proxy for the degree of interaction between nanotubes in the composite in its unstrained state. The sensitivity of a strain sensor is characterized by quantity known as the gauge factor (G), which is defined as:

$$G = \frac{\frac{R-R_0}{R_0}}{\varepsilon} = \frac{\Delta R/R_0}{\varepsilon} \quad (2)$$

where ε is the applied strain, R and R_0 are the resistance of the sensor at $\varepsilon = 0$ and ε , and $\Delta R/R_0$ is the normalized resistance change. As shown in Figure 4, the normalized

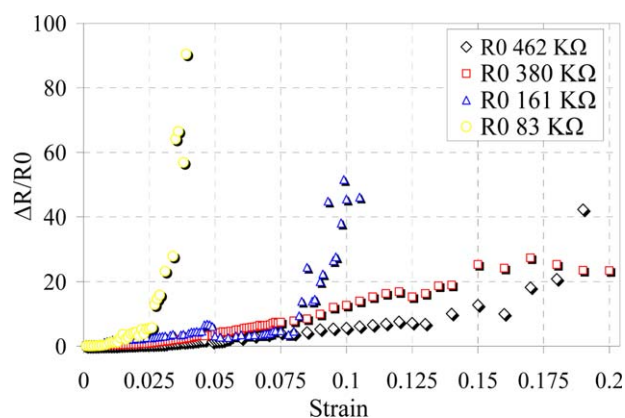


FIGURE 4 The strain versus normalized resistance change of the MWCNT/PDMS sensors with different initial resistances (R_0). [Color figure can be viewed in the online issue, which is available at wileyonlinelibrary.com.]

resistance change of four samples displays similar monotonic increase with the increase of strain. For two sensors with a higher R_0 , they exhibit a linear strain-normalized resistance change in the small strain range ($0 < \varepsilon < 2.5\%$), with calculated gauge factors of 20 ($R_0 = 462$ k Ω) and 32 ($R_0 = 380$ k Ω), respectively (Fig. 5). Under a higher strain range (2.6–14%), nonlinearity appeared. When strain was released, the resistances of these two sensors were immediately restored to 420 and 590 k Ω , and further reduced to 390 and 450 k Ω after 4 h, which indicated that microlines were not permanently deformed or damaged during the sensing process. The delay of the recovery of the resistance is likely due to the viscoelasticity of the PDMS, as the stress relaxation of strained PDMS molecular chains is a dynamic process to reach the equilibrium. Sensors with lower initial resistance (83 and 161 k Ω) exhibited much higher piezoresistivity values than these with the higher R_0 , as indicated by different slopes of the curves in Figures 4 and 5. Compared to sensors

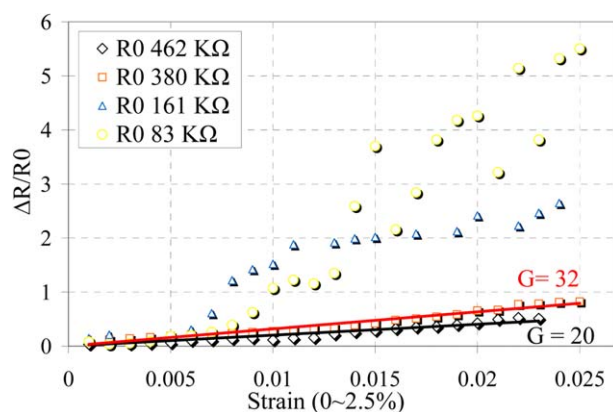


FIGURE 5 Piezoresistive responses of MWCNT/PDMS sensors at the small strain range (0–2.5%). [Color figure can be viewed in the online issue, which is available at wileyonlinelibrary.com.]

with a higher R_0 , composites with lower R_0 exhibited more pronounced nonlinearity. Dang et al. has reported very similar nonlinear piezoresistive behaviors of a silicone rubber/MWCNTs pressure sensor.¹² The degradation of linearity may be partially attributed to the pullout of concentric graphene tubes of a MWCNT.¹⁴ The high R_0 samples have less load transfer to the individual CNT to allow the pullout to occur efficiently.

As the sensor sensitivity demonstrated a strong dependence on both the R_0 and the ε , a detailed analysis was conducted in an effort to elucidate the sensing mechanisms of MWCNT/PDMS composite. To this end, six sensors with a variety of R_0 were fabricated and their sensitivities were evaluated. The typical curve of the normalized resistance change versus applied strain exhibited three distinct regions as shown in Figure 6. In region I where the applied strain ranges from 0 to 1%, $\Delta R/R_0$ increases linearly with the strain, so the gauge factor is the slope of the linearly fitted curve in this region according to eq (2), and is referred as G_1 . In region II and III, in which the applied strains ranges were 1–2 and 2–10%, the curve shows different degrees of nonlinearity. To study the G as a function of the strain, the values of the G at the strain of 2 and 10% were calculated separately using eq (2), and were referred as G_2 and G_3 in Figures 6 and 7. In some low R_0 samples, the material failed at the strain less than 1%, therefore, G_2 or G_3 are not available for these sensors. The gauge factor of each sensor under each of the aforementioned three strain regions was plotted in Figure 7. It is observed that the gauge factor of all tested devices increases consistently with the increase of applied strain level. In the three strain levels, the sensitivity of each sensor first drops with increased R_0 when R_0 is below a certain value and then started to increase when R_0 is above a certain value.

Piezoresistive Effects in MWCNT/PDMS Composites

To elucidate the piezoresistive behavior observed in Figures 6 and 7, it is necessary to investigate the general mecha-

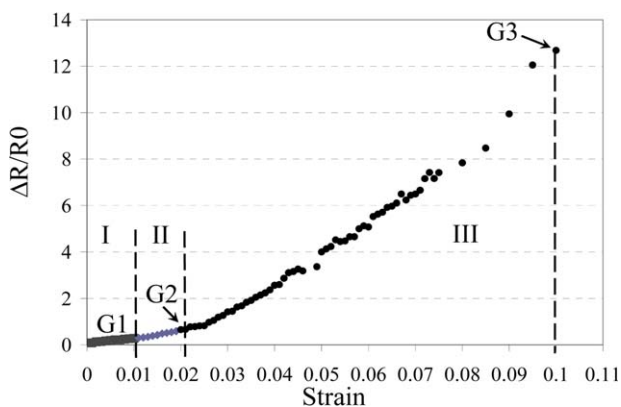


FIGURE 6 The typical curve of the normalized resistance change versus the applied strain of the MWCNT/PDMS composites. [Color figure can be viewed in the online issue, which is available at wileyonlinelibrary.com.]

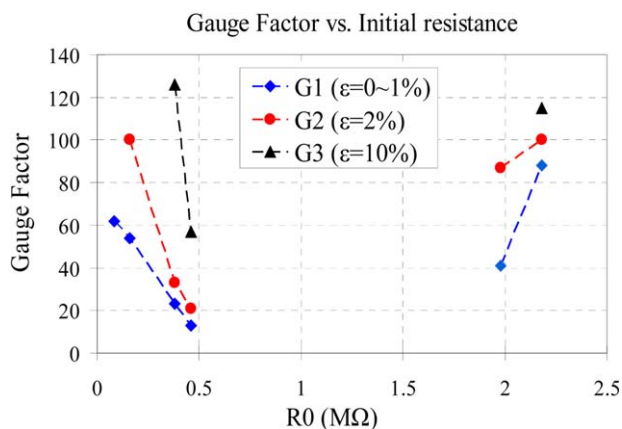
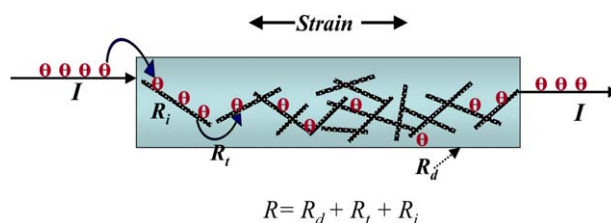


FIGURE 7 The gauge factor (G) as a function of the initial resistance (R_0) of the sensor and the applied strain range (ε) (G_1 , G_2 , and G_3 are gauge factors at three different strain regions shown in Fig. 6). [Color figure can be viewed in the online issue, which is available at wileyonlinelibrary.com.]

nisms of the piezoresistivity in a MWCNT/PDMS composite. In contrast to metal, the total resistance of a MWCNT/PDMS microline is attributed to three factors, as illustrated in Figure 8. When electrons are injected into the composite, they first need to overcome the intrinsic resistivity of the individual tube (R_i). When they reach the end of the CNT, the energy barrier associated with the tunneling resistance (R_t) between two adjacent CNTs need to be overcome to allow electrons to move forward in the CNT network. Meanwhile, the resistance arising from the geometry of a conductor adds up to the total resistance (R_d). When a tensile strain is applied to this structure, R_d , R_t , and R_i change accordingly due to the alternation of the dimension, the distance between two adjacent CNTs, and the length/geometry of an individual CNT. Consequently, three piezoresistive mechanisms can contribute to the overall sensitivity, which are referred as G induced by the dimensional change (G_d), G induced by the alternation of tunneling resistance (G_t) and G induced by the modification of CNT bandgap (G_i). The total piezoresistivity (G) is thereby the result of all three effects. Each type of the gauge factors can be mathematically quantified as follows:

1. when a conductor is incompressible, piezoresistivity caused by the dimensional change of a conductive line, G_d , is calculated by the following equation:



$$R = R_d + R_t + R_i$$

FIGURE 8 Scheme of electron transportation in a MWCNT/PDMS composite. [Color figure can be viewed in the online issue, which is available at wileyonlinelibrary.com.]

$$G_d = \frac{R_1 - R_0}{\varepsilon} = \frac{\rho l_0 \frac{(1+\varepsilon)}{A} - \rho \frac{l_0}{A_0}}{\varepsilon \rho \frac{l_0}{A_0}} = \varepsilon + 2 \quad \rho A l = \rho A l (1+\varepsilon) = \rho A_0 l_0 \quad (3)$$

where ρ is the density of the microline, l and l_0 are the strained and unstrained length of the microline, A and A_0 are the strained and unstrained cross-sectional area, ε is the applied tensile strain, and R_1 and R_0 are the resistances at ε and the zero strain, respectively. Equation (3) indicates that the G_d increases linearly with the applied strain. As the working range in most strain sensors is less than 15%, the gauge factor of this type of sensors is limited to 2.15, which is consistent with most of the reported metal foil strain gauges.⁴

2. The piezoresistivity induced by the change of the tunneling resistance and the total number of conductive paths in a composite, G_t , can be approximated as^{15–19}:

$$G_t = \frac{R(\varepsilon) - R_0}{\varepsilon} = \frac{\exp(2\alpha d_0 \varepsilon) - 1}{\varepsilon} \quad (4)$$

$$\alpha = \frac{2\pi}{h} (2m\varphi)^{1/2} \quad (5)$$

where $R(\varepsilon)$ and R_0 are the resistance at the strain of ε and 0, d_0 is the tunneling distance between CNTs, h is the Planck's constant, m is the mass of the charge carriers, and φ is the height of the tunneling barrier.

G_t increases nonlinearly and monotonically with applied strain. In addition, because the resistance changes under the strain will be more pronounced when the total number of conductive paths in the composite decreases, G_t has been reported to increase with increased R_0 .^{20–22} Therefore, the piezoresistive effect becomes more pronounced when the concentration of CNTs distributed in a polymer matrix approaches the percolation threshold.

3. The gauge factor arising from a strained individual CNT, G_i , obeys the following relationship²⁴:

$$G_i = \frac{\exp\left(\frac{E_g(\varepsilon)}{k_B T}\right) - \exp\left(\frac{E_g(\varepsilon=0)}{k_B T}\right)}{\left[1 + \exp\left(\frac{E_g(\varepsilon=0)}{k_B T}\right)\right]} \cdot \frac{1}{\varepsilon} \quad (6)$$

where $E_g(\varepsilon)$ is the strain-dependent band gap of a metallic nanotube (torsion contributions are neglected) and $E_g(\varepsilon) = \left(\frac{dE_g}{d\varepsilon}\right) \cdot \varepsilon$. k_B is the Boltzmann constant, and T is the temperature. Similarly to G_t , G_i exhibits a nonlinear relationship with the applied strain, with a high gauge factor ranging from 200 to 2900.^{23,24}

Thickness Dependence on the Initial Resistance

As plotted in Figure 9, the R_0 of the MWCNT/PDMS sensors decreases nonlinearly with increased CNT layer thickness (d), which is likely due to the increased number of conductive paths within a CNT network when the CNT layer becomes

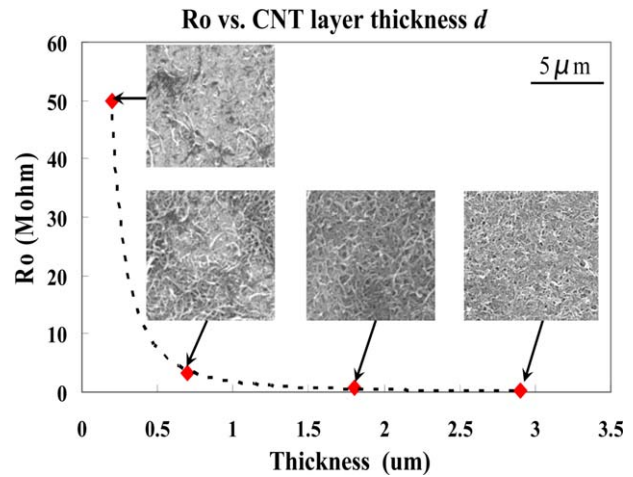


FIGURE 9 The R_0 as a function of the CNT layer thickness in MWCNT/PDMS sensors. Inserted SEM images: morphology of CNT films with the different R_0 . [Color figure can be viewed in the online issue, which is available at wileyonlinelibrary.com.]

thicker.²⁴ The percolation threshold of the composite is reached when the CNT layer thickness is approximately 400–500 nm. When d reduces to the value well below the percolation point (e.g., $d < 200$ nm), the R_0 increases rapidly and eventually become infinite. The composite therefore becomes nonconductive due to lack of entanglement/contact of CNTs in the network evidenced by the SEM images in Figure 9.

Interpretation of the Piezoresistive Behaviors of the MWCNT/PDMS Strain Sensors

Combining the discussions in Piezoresistive Effects in MWCNT/PDMS Composites and Thickness Dependence on the Initial Resistance sections, it is reasonable to speculate that all three piezoresistive mechanisms were present and coupled in the strained MWCNT nanocomposite, while the magnitude of each effect could be different as R_0 varied. The following explanations and conclusions of the piezoresistive behavior of the sensor were made:

1. When the R_0 of the strain sensor was less than 500 k Ω , the CNT layer thickness was found to be greater than 1 μm (Fig. 9). Because the diameter of an individual CNT is approximately 50–80 nm, the layer was composed of approximately 15 layers of CNTs. These layers formed a dense and interpenetrating conductive network and the CNT concentration was well above the percolation point. As a result, it is reasonable to assume that in this R_0 range where the CNT layer is sufficiently thick, the piezoresistive mechanism may be primarily attributed to the intrinsic CNT piezoresistivity (G_i) and the dimensional change induced piezoresistivity (G_d). The CNT layer in the device configuration is in direct contact with the stretch frame and the network is highly entangled, the force can therefore be directly transferred within the CNT network and subsequently deform the tubes. This is opposed to the case where CNTs are loosely embedded deep inside a

polymer matrix and the load transfer from the polymer to the CNTs is insufficient to deform the individual CNTs because CNT has a much higher Young's modulus (~ 1 TPa) than PDMS (~ 2 MPa). To verify the assumption that the individual CNT was deformed in this R_0 range, a Raman study was conducted. As shown in Figure 10, both the 2D band and the G band exhibited increased blue shift with the higher strain, which indicates the individual CNT was strained.^{25–28} The gauge factor in this R_0 range varies from 13 to 120 (Fig. 7), which is close to the theoretically predicted and experimentally obtained values as discussed in part (iii) of Piezoresistive Effects in MWCNT/PDMS Composites section. The higher G observed in composites with a lower R_0 in this range is likely due to the larger stress that a thicker CNT layer experienced than the thinner one under the same strain due to the higher Young's modulus present in a thicker CNT layer,²⁸ which subsequently leads to a bigger change of the CNT bandgap (eq (6)). The phenomenon is consistent with the piezoresistive behavior induced by intrinsic piezoresistivity.^{28–30} The increased gauge factor induced by a higher strain is also well aligned with the theoretical prediction by eq (6).

2. When R_0 is above $1.9 \text{ M}\Omega$, the CNT layer thickness reduces to below 600 nm (Fig. 9). Morphology studies confirm that the composite in this R_0 range approaches the percolation point. CNTs are observed to be loosely packed, forming a sparsely entangled interpenetrating network within the PDMS matrix. In this case, the majority of the deformation likely takes place in the PDMS phase as the Young's modulus of PDMS is six orders of magnitude lower than that of the CNT. The resistance change due to the deformation of an individual CNT could therefore be minimal because of the insufficient load transfer from the soft PDMS phase to the rigid CNT phase. Thereby, the piezoresistivity induced by the change of the tunneling resistance, G_t , should play the dominant role. The gauge factor in this R_0 range is found to be approximately 40–120, which is well aligned with the theoretically modeled values using eq (4). In contrast to the G induced by the intrinsic piezoresistivity of a CNT as discussed in (1), the

gauge factor in this mechanism increases with R_0 , which is the characteristic of the piezoresistivity induced by the tunneling resistance discussed in Piezoresistive Effects in MWCNT/PDMS Composites section. These observations confirm that the alteration of the tunneling resistance is likely to be the primary cause for the piezoresistivity of the sensors in this R_0 range.

3. The multiple regions of the gauge factors observed in this work should be primarily attributed to the different degree of the effects of the three mechanisms present in the different strain levels. At the small strain level, the percolation-based piezoresistivity dominates. While at the high strain level, individual CNT is also strain in addition to the tunneling effects, therefore, a higher piezoresistivity is observed. Similar strain dependence was also reported by other peers.^{31,32}

HYSTERESIS STUDY OF THE PDMS/CNTs STRAIN SENSOR

The sensor shows a good resistance recovery when strain is released, as indicated by Figure 11. A certain degree of hysteresis was also observed, where slight deviations occurred in the unloading curve from the loading curves. The issue is less pronounced in the low strain range ($\epsilon < 2.5\%$). Such phenomenon is common in most carbon nanotube-loaded elastomer systems,^{33,34} which may be partially due to the viscoelasticity of polymer matrix. Studies of the same type of PDMS (Sylgard 184, Dow Corning) have shown the presence of hysteresis under cyclic mechanical deformation.³⁵ However, due to the complex nature of the nanocomposite and given the fact that hysteresis could have three sources including PDMS, CNTs, and their composite form, further investigation is needed for a more accurate explanation.

CONCLUSIONS

Complex 2D/3D MWCNT/PDMS composite patterns with controllable CNT layer thickness were achieved using the MEMS-assisted EPD technique. The developed sensors demonstrated high sensitivities to the tensile strain with gauge factors ranging from 13 to 120. The gauge factor shows a

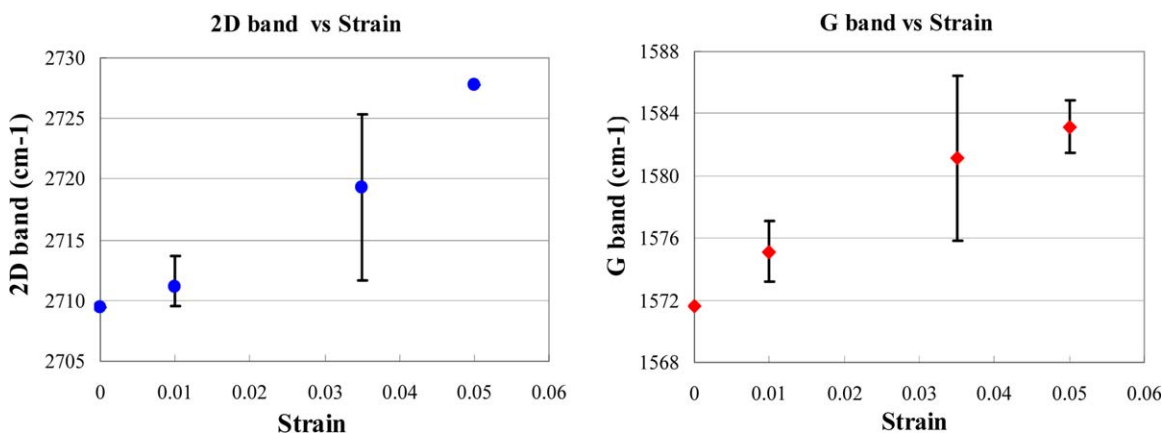


FIGURE 10 Raman shift of the 2D band (left) and the G band (right) of the unstrained and strained MWCNT/PDMS composites. [Color figure can be viewed in the online issue, which is available at wileyonlinelibrary.com.]

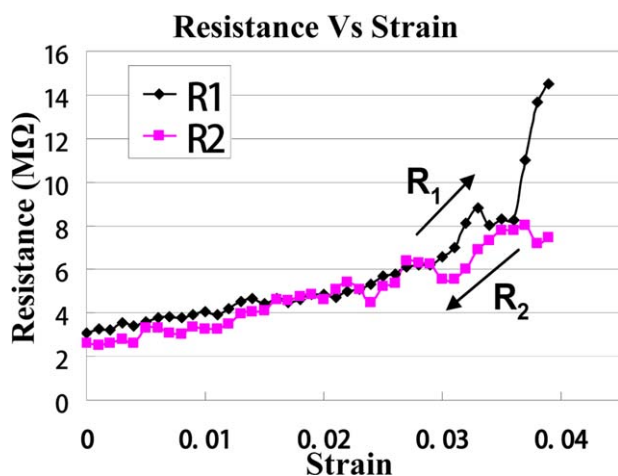


FIGURE 11 Hysteresis of the resistance response upon strain of the PDMS/CNT nanocomposite. [Color figure can be viewed in the online issue, which is available at wileyonlinelibrary.com.]

strong dependence on both the initial resistance of the sensor and the applied strain. Depending on the morphology and the thickness of the CNT network, different piezoresistive mechanisms play the dominant role. When the entanglement of CNTs in a network is sufficient to allow effective load transfer between them, sensitivity of the sensor is likely dominated by the intrinsic piezoresistivity of the individual CNT. Conversely, when CNTs are loosely dispersed in the polymer matrix, piezoresistivity associated with the tunneling resistance is the most significant contribution to the device sensitivity. Because the R_0 can be modulated by the patterning technique, the gauge factor of the sensor can be approximately predicted using the MEMS-assisted EPD approach. It also enables detailed study of the sensing mechanism. The work provides useful guidance for the design and fabrication of the strain/stress sensors with a specific sensitivity. Compared with traditional metal foil strain sensors ($G = 2.1$) and silicon piezoresistors ($G < 120$), the patternable MWCNT/PDMS composite exhibits comparable or much higher strain sensitivity, with additional advantages of a larger working range ($>10\%$) and the mechanical flexibility. The composite developed herein can potentially be utilized to sense and monitor the local pressure and structural change in tissues, microfluidic systems, as well as flexible 3D Microsystems.

REFERENCES AND NOTES

- 1 T. Yamada, Y. Hayamizu, Y. Yamamoto, Y. Yamogida, K. Hata, *Nat. Nanotechnol.* **2011**, *6*, 296–301.
- 2 O. Yilmazoglu, A. Popp, D. Pavlidis, J. Schneider, F. Schüttler, G. Battenberg, *Nanotechnology* **2012**, *23*, 085501.
- 3 L. Chen, G. H. Chen, L. Liu, *Adv. Funct. Mater.* **2007**, *17*, 898–904.
- 4 P. Alpuim, C. Costa, *J. Non-Cryst. Solids* **2008**, *354*, 354: 2585–2589.
- 5 M. Tabib-Azar, R. Wang, Y. Xie, L. You, In Proceedings of the 1st IEEE International Conference on Nano/Micro Engineered and Molecular Systems, Zhuhai, China **2006**; pp 1297–1302.

- 6 N. White, A. Cranny, *Microelectron. Int.* **1987**, *4*, 32–35.
- 7 J. Cao, Q. Wang, H. Dai, *Phys. Rev. Lett.* **2003**, *90*, 157601.
- 8 H. S. Nalwa, *Nanostructured Materials and Nanotechnology*; Academic Press: San Diego, **2002**.
- 9 W. J. Xu, C. H. Ji, R. Shafer, M. G. Allen, In Proceedings of Materials Research Society Conference **2009**; *1139*, No.: 1139-GG03–06.
- 10 W. J. Xu, M. G. Allen, In Tech. Dig. Int. Solid-State Sensors, Actuators and Microsystems Conference - TRANSDUCERS **2009**; pp 2242–2245.
- 11 H. C. Hamaker, *Trans. Faraday Soc.* **1940**, *35*, 279–287.
- 12 Z. M. Dang, D. Xie, S. H. Yao, L. Q. Zhang, J. Bai, *J. Appl. Phys.* **2008**, *104*, 024114(1–6).
- 13 J. L. Rigueur, Ph.D. Thesis, **2012**, Multi-walled Carbon Nanotube Films: Fabrication Techniques and Applications, Vanderbilt University.
- 14 M. Olek, J. Ostrander, S. Jurga, H. Möhwald, N. Kotov, K. Kempa, M. Giersig, *Nano Lett.* **2004**, *4*, 1889–1895.
- 15 I. Kang, J. Kim, *Smart Mater. Struct.* **2006**, *15*, 737.
- 16 J. G. Simmons, *J. Appl. Phys.* **1963**, *34*, 1793–1804.
- 17 C. J. Adkins, *J. Phys.: Condens. Matter* **1989**, *1*, 1253–1260.
- 18 T. A. Ezquerra, M. Kuleszcza, C. S. Cruz, F. J. Baltá-Calleja, *Adv. Mater.* **1990**, *2*, 597–600.
- 19 F. M. Du, R. C. Scogna, W. Zhou, S. Brand, J. E. Fischer, K. I. Winey, *Macromolecules* **2004**, *37*, 9048–9055.
- 20 J. H. Kang, C. Park, J. A. Scholl, A. H. Brazin, N. M. Holloway, J. W. High, S. E. Lowther, and J. S. Harrison, *J. Polym. Sci. Part B: Polym. Phys.* **2009**, *47*, 994–1003.
- 21 C. Gao, H. S. Ko, H. T. Chen, *Nanotechnology* **2009**, *20*, 185503.
- 22 J. R. Bautista-Quijano, F. Avilés, J. O. Aguilar, A. Tapia, *Sensors Actuat. A-Phys.* **2010**, *159*, 135–140.
- 23 C. Stampfer, T. Helbling, D. Oberfell, B. Schöberle, M. K. Tripp, A. Jungen, S. Roth, V. M. Bright, C. Hierold, *Nano Lett.* **2006**, *6*, 233–237.
- 24 M. J. O’Connell. *Carbon Nanotubes: Properties and Applications*. Taylor & Francis Group, LLC CRC Press; **2006**.
- 25 L. S. G. Schadler, P. M. Ajayan, *Appl. Phys. Lett.* **1998**, *73*, 3842–3844.
- 26 W. K. Qiu, Z. K. Lei, Q. H. Qin, Q. Li, Q. A. Wang, *J. Raman Spectrosc.* **2010**, *41*, 1216–1220.
- 27 P. W. Y. Barone, R. Ortiz-Garcia, J. Q. Zhang, J. H. Ahn, J. H. Kim, M. S. Strano, *Acs Nano* **2009**, *3*, 3869–3877.
- 28 K. J. Loh. *Development of Multifunctional Carbon Nanotube Nanocomposite Sensors for Structural Health Monitoring*. Ann Arbor, MI, USA, University of Michigan, Ph.D. Dissertation, **2008**.
- 29 K. Lee, S. S. Lee, J. A. Lee, K. C. Lee, S. Ji, *Appl. Phys. Lett.* **2010**, *96*, 013511.
- 30 X. H. Song, Z. Y. Gan, Q. Lv, H. Cao, H. Yan, *Microelectron. Eng.* **2009**, *86*, 2330–2333.
- 31 B. R. Loyola, V. L. Saponara, K. J. Loh, *J. Mater. Sci.* **2010**, *45*, 6786–6798.
- 32 M. Park, H. Kim, J. P. Youngblood, *Nanotechnology* **2008**, *19*, 055705.
- 33 C. X. Liu, J. W. Choi, *IEEE Trans. Nanotechnol.* **2010**, *9*, 590.
- 34 L. Ci, J. Suhr, V. Pushparaj, X. Zhang, P. M. Ajayan, *Nano Lett.* **2008**, *8*, 2762.
- 35 Y. P. Khanna, T. J. Taylor, V. V. Vickroy, R. F. Abbott, *Macromolecules* **1985**, *18*, 1302.